A Theoretical and Experimental Framework for Understanding Electrogenerated Chemiluminescence (ECL) Emission at Bipolar Electrodes

ARTICLE *in* ANALYTICAL CHEMISTRY · AUGUST 2009

Impact Factor: 5.64 · DOI: 10.1021/ac900744p · Source: PubMed

6 AUTHORS, INCLUDING:

François Mavré
Paris Diderot University
34 PUBLICATIONS **607** CITATIONS
SEE PROFILE

Kwok-Fan Chow
University of Massachusetts Lowell
13 PUBLICATIONS **416** CITATIONS
SEE PROFILE

Anal. Chem. **2009,** *81,* 6218–6225

A Theoretical and Experimental Framework for Understanding Electrogenerated Chemiluminescence (ECL) Emission at Bipolar Electrodes

François Mavré, Kwok-Fan Chow, Eoin Sheridan,† Byoung-Yong Chang, John A. Crooks, and Richard M. Crooks*

Department of Chemistry and Biochemistry and the Center for Electrochemistry, The University of Texas at Austin, 1 University Station, A5300, Austin, Texas 78712-0165

Bipolar electrodes are potentially useful for a variety of sensing applications, but their implementation has been hampered by an inability to easily monitor the current through such electrodes. However, current can be indirectly determined using electrogenerated chemiluminescence (ECL) as a reporting mechanism. This paper provides a detailed theoretical analysis of ECL reporting at bipolar electrodes. In addition, experiments are described that confirm the theory. Finally, we correlate ECL intensity directly to current through the use of split bipolar electrodes. The results indicate that the lowest current that can be indirectly detected through ECL reporting is ~32 μA/cm², which corresponds to a reporting sensitivity of ~7200 counts/nA in the present experimental system.

In this report, we show how the magnitude of the electrogenerated chemiluminescence (ECL) emission at a floating, bipolar electrode relates to the current flowing through the electrode. This correlation presents an experimental challenge, because bipolar electrodes lack external connections. We address this problem using electrode configurations that mimic the behavior of bipolar electrodes, and a rigorous, quantitative analysis of the results makes it possible to determine the emission efficiency of bipolar electrodes. This detailed level of understanding is essential for future analytical applications of bipolar electrode arrays.[1−5]

Scheme 1

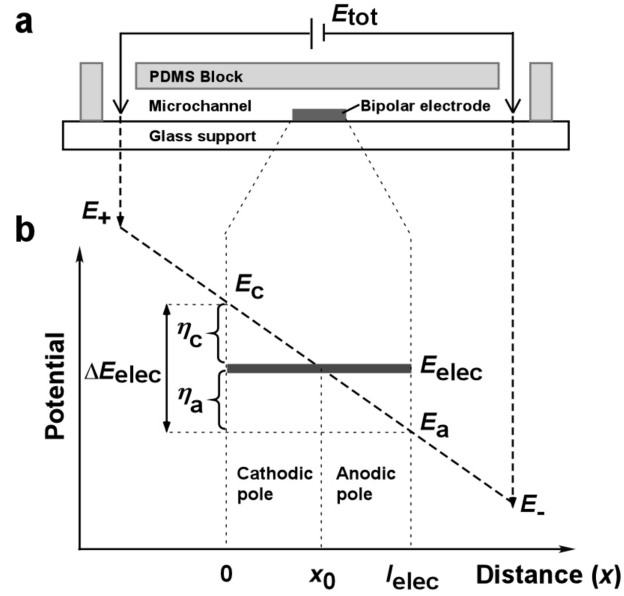

We and others previously demonstrated that an isolated, conductive wire placed within a microfluidic channel can act as a bipolar electrode when a sufficiently high potential difference is applied across the solution that contacts the electrode.[1−14] Scheme 1 illustrates this principle. It is important to note that we assume a linear electric field, because, as will be discussed later, ~99% of the total current passes through the electrolyte solution, rather than through the bipolar electrode. Therefore, distortion of the electric field by faradaic current is negligible.

* To whom correspondence should be addressed. Tel.: 512-475-8674. E-mail: crooks@cm.utexas.edu.

† Present address: National Centre for Sensor Research, School of Chemical Sciences, Dublin City University, Dublin 9, Ireland.

(1) Arora, A.; Eijkel, J. C. T.; Morf, W. E.; Manz, A. *Anal. Chem.* **2001**, *73*, 3282–3288.
(2) Zhan, W.; Alvarez, J.; Crooks, R. M. *J. Am. Chem. Soc.* **2002**, *124*, 13265–13270.
(3) Zhan, W.; Alvarez, J.; Crooks, R. M. *Anal. Chem.* **2003**, *75*, 313–318.
(4) Zhan, W.; Alvarez, J.; Sun, L.; Crooks, R. M. *Anal. Chem.* **2003**, *75*, 1233–1238.
(5) Chow, K. F.; Mavré, F.; Crooks, R. M. *J. Am. Chem. Soc.* **2008**, *130*, 7544–7545.
(6) Fleischmann, M.; Ghoroghchian, J.; Rolison, D.; Pons, S. *J. Phys. Chem.* **1986**, *90*, 6392–6400.
(7) Klett, O.; Nyholm, L. *Anal. Chem.* **2003**, *75*, 1245–1250.
(8) Ordeig, O.; Godino, N.; del Campo, J.; Munoz, F. X.; Nikolajeff, F.; Nyholm, L. *Anal. Chem.* **2008**, *80*, 3622–3632.
(9) Ulrich, C.; Andersson, O.; Nyholm, L.; Björefors, F. *Angew. Chem., Int. Edit.* **2008**, *47*, 3034–3036.
(10) Ulrich, C.; Andersson, O.; Nyholm, L.; Björefors, F. *Anal. Chem.* **2009**, *81*, 453–459.
(11) Duval, J.; Kleijn, J. M.; van Leeuwen, H. P. *J. Electroanal. Chem.* **2001**, *505*, 1–11.
(12) Duval, J. F. L.; Minor, M.; Cecilia, J.; van Leeuwen, H. P. *J. Phys. Chem. B* **2003**, *107*, 4143–4155.
(13) Duval, J. F. L.; van Leeuwen, H. P.; Cecilia, J.; Galceran, J. *J. Phys. Chem. B* **2003**, *107*, 6782–6800.
(14) Duval, J. F. L.; Sorrenti, E.; Waldvogel, Y.; Görner, T.; De Donato, P. *Phys. Chem. Chem. Phys.* **2007**, *9*, 1713–1729.
(15) Noffsinger, J. B.; Danielson, N. D. *Anal. Chem.* **1987**, *59*, 865–868.
(16) Leland, J. K.; Powell, M. J. *J. Electrochem. Soc.* **1990**, *137*, 3127–3131.
(17) Miao, W. J. *Chem. Rev.* **2008**, *108*, 2506–2553.

10.1021/ac900744p CCC: $40.75
Published on Web 07/02/2009

Our present system consists of a simple PDMS microfluidic channel that houses a microfabricated gold electrode (see Scheme 1a). When an electric field is generated inside the channel by supplying a potential between two "driving" electrodes at either end of the channel, faradaic reactions can occur at the gold electrode/solution interface. The reason for this behavior is that the fraction of the potential dropped in the solution along the electrode causes an interfacial potential difference that varies laterally along the electrode (see Scheme 1b). This leads to an electrochemical reduction at the cathodic pole of the electrode and an oxidation at the anodic pole.[6] Because electroneutrality must be satisfied within the bipolar electrode, the oxidation and reduction reactions are balanced and occur simultaneously.

Our group and others have previously demonstrated that bipolar electrochemistry in a microfluidic environment can be used to build wireless sensors.[1−5] Manz and co-workers[1] were the first to introduce the idea of using wireless electrochemical detection in a separation system. They used a microfluidic channel housing a floating, U-shaped platinum electrode for the detection of various amino acids in the presence of $Ru(bpy)_3^{2+}$. In their system, the amino acids acted as coreactants for $Ru(bpy)_3^{2+}$ ECL at the anodic pole of the bipolar electrode.

Our group developed an alternative microchip ECL detection strategy at approximately the same time as the Manz discovery.[2−5] While the Manz approach was limited to detection of coreactants for $Ru(bpy)_3^{2+}$-based ECL (typically molecules bearing amine functionalities),[15−17] our approach could be used to detect any electrochemically active analyte. Specifically, we determined that the reduction of an analyte at the cathodic pole of a bipolar electrode could be related to an ECL process at the anodic pole. The interesting aspect of this finding is that the sensing and ECL reporting events are chemically decoupled; that is, the analyte and the light-emitting species do not interact chemically. We recently extended this strategy to the detection of DNA at an array of bipolar electrodes contained within a microfluidic channel.[5] In this experiment, cDNA labeled with platinum nanoparticles was recruited to the cathodic pole of a bipolar electrode previously functionalized with probe DNA. Once in the vicinity of the bipolar electrode, the platinum nanoparticle catalyzed the reduction of O_2. Because O_2 reduction at the cathode end of the bipolar electrode is electrically coupled to ECL emission at the anode end, light is emitted from the bipolar electrode only in the presence of the DNA target. The significant outcome of this study is its demonstration that large electrode arrays can be used to simultaneously detect the presence of biological molecules without making direct electrical contact with each electrode in the array.

Nyholm and co-workers[7,8] recently reported on an electrochemical detection scheme using a strategy related to that reported here. They recognized that two individual electrodes could be connected outside of a fluidic channel and thus act as a single bipolar electrode. More importantly, by connecting an ammeter between the two electrodes, they were able to measure current directly. The Nyholm group has also reported a measure of the potential and current density distribution at the bipolar electrode/solution interface.[9,10]

Duval and co-workers[11−14] previously studied the fundamental principles of bipolar electrochemistry in an effort to better understand unanticipated behavior related to corrosion[11] and streaming potentials.[12] They created a rigorous mathematical model to describe the distribution of overpotential and current density along a planar bipolar electrode in an electric field. They also confirmed their model experimentally by monitoring the anodic dissolution of an aluminum bipolar electrode in an applied electric field.[11]

The principal objective of the present paper is to compare the sensitivity of light-based ECL detection with a direct measurement of the faradaic current passing through a bipolar electrode quantitatively. This comparison provides a more complete understanding of the fundamental properties of bipolar electrodes, particularly as they relate to electroanalytical chemistry, a direct measure of the relative sensitivity of the two detection methods, and a theoretical framework for optimizing biosensors based on bipolar electrode arrays.

EXPERIMENTAL SECTION

Chemicals. $Ru(bpy)_3Cl_2 \cdot 6H_2O$ (bpy = 2,2′-bipyridine) (224758) and tri-*n*-propylamine (TPrA, 239712) were purchased from Strem Chemicals and Sigma−Aldrich, respectively, and used as received, unless otherwise noted in the text. Milli-Q water (Milli-Q reagent water system, Millipore, Bedford, MA) was used to prepare all aqueous solutions.

Device Fabrication. Standard lithographic methods were used to prepare the gold electrodes on glass slides and the poly(dimethylsiloxane) (PDMS) microfluidic channels for the microfluidic devices.[18] Detailed information is provided in the Supporting Information. The dimensions of the channel were as follows: length, 1.2 cm; width, 1.75 mm; and height, 28 μm. A hole puncher with a diameter of 1.0 mm was used to form the reservoirs at the two ends of the microchannel. The length of the bipolar electrodes was 1.00 mm. Each half of the split bipolar electrode design was 450 μm long, and they were separated by 100 μm.

Luminescence Micrographs. A microscope (Nikon AZ100, Nikon Co., Tokyo, Japan) that was equipped with a mercury lamp (Nikon) and a CCD camera (Cascade, Photometrics, Ltd., Tucson, AZ) were used to obtain the optical and luminescence micrographs. The luminescence micrographs were obtained under darkroom conditions, with an exposure time of 1500 ms. Micrographs were processed using V++ Precision Digital Imaging software (Digital Optics, Auckland, New Zealand).

Note that the intensity of the ECL emission for a given driving potential stabilized only after the second scan (devices were scanned several times from 0 V to 23 V, and only the third scan is reported). Black deposits were observed for some devices in the vicinity of location of the light emission. Control experiments have shown that the deposits correlate with the oxidation of $Ru(bpy)_3^{2+}$. The deposits can be removed from the electrode by flushing the channel with electrolyte solution.

RESULTS AND DISCUSSION

Principles and Theoretical Considerations. The configuration of the bipolar electrode and microfluidic system used in these experiments is shown in Scheme 1a. The design is similar to that used in a previous report from our group.[5] It is comprised

(18) Xia, Y.; Whitesides, G. M. *Angew. Chem., Int. Edit.* **1998**, *37*, 550–575.

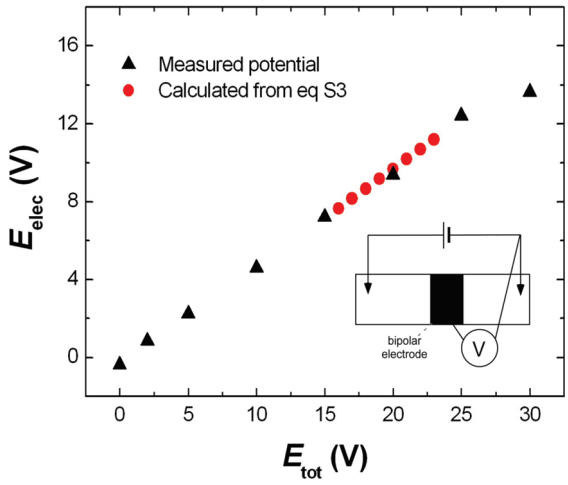

Figure 1. Potential of the bipolar electrode (E_{elec}) as a function of the applied driving voltage (E_{tot}). The solution contained 5.0 mM $Ru(bpy)_3^{2+}$ and 25.0 mM TPrA in 0.100 M phosphate buffer (pH 6.9). The inset shows an illustration of the experimental setup used to conduct these measurements (see the Supporting Information for details).

of a gold electrode (1.00 mm × 0.25 mm) configured at the center of a microfluidic channel. The channel contains a solution that consists of 5.0 mM $Ru(bpy)_3^{2+}$ and 25.0 mM TPrA in 0.100 M phosphate buffer (pH 6.9).

When a potential E_{tot} is applied between two driving electrodes situated in reservoirs at either end of the microchannel, the majority of E_{tot} is dropped in the microchannel, because of the high solution resistance within the channel (see Scheme 1b). Hence, if we assume that the potential drop at the driving electrode/solution interface and within the reservoirs is negligible, then the resulting electric field (V_0) inside the channel is given by $V_0 = (E_{tot}/l_{channel})$. Here, V_0 is assumed to be constant throughout the entire length of the channel.

When a bipolar electrode is placed inside this microchannel, a fraction of E_{tot}, denoted as ΔE_{elec}, is dropped across its length, l_{elec} (see eq 1).

$$\Delta E_{elec} = E_c - E_a = V_0 \times l_{elec} = \frac{E_{tot}}{l_{channel}} \times l_{elec} \qquad (1)$$

Here, E_c represents the solution potential over the bipolar electrode at $x = 0$ and E_a is the solution potential where $x = l_{elec}$. The potential of the bipolar electrode floats, which means that it is not controlled against a reference value. Accordingly, the potential of the bipolar electrode (E_{elec}) will adjust to the surrounding solution potential. Moreover, because the electrode surface experiences a continuum of solution potentials ranging from E_c to E_a, the electrode potential will adjust to an equilibrium value (E_{elec}) situated between E_c and E_a. Measured and calculated values of the bipolar electrode potential are plotted in Figure 1. Additional information about how this experiment was conducted, and how the data were analyzed, are provided in the Supporting Information.

Position x_0 (see Scheme 1b) is defined as the particular location where the potential of the solution is equal to E_{elec}. Accordingly, the electrode is divided into two poles: a cathodic pole ($x < x_0$) and an anodic pole ($x > x_0$). For both the cathodic and anodic poles, the difference in potential between the electrode and the solution at any location x is $\eta_{(x)}$, which is the driving force that leads to an electrochemical reduction or oxidation, respectively. Because the electric field is considered constant throughout the channel, η varies linearly as a function of x across the electrode surface (see eq 2).

Scheme 2

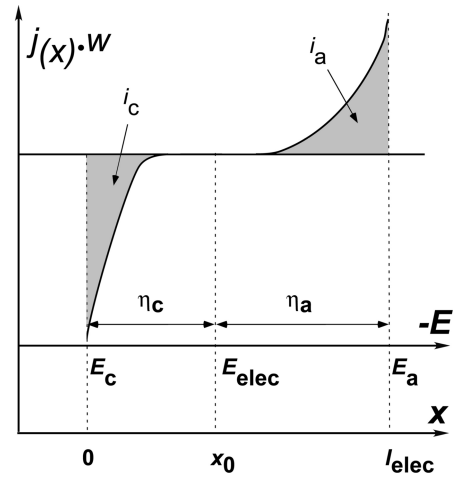

$$\eta_{(x)} = E_{elec} - E_{(x)} = V_0(x_0 - x) = \frac{\Delta E_{elec}}{l_{elec}}(x_0 - x) \qquad (2)$$

The variation of $\eta_{(x)}$ with distance across the bipolar electrode implies that the current density ($j(x)$) at the metal/solution interface is also a function of distance. The current density profile is dependent on both the thermodynamic and kinetic characteristics of the electrochemical processes occurring at the cathodic and anodic poles (here, the reduction of oxygen and water, and the oxidation of $Ru(bpy)_3^{2+}$ and TPrA, respectively).

Scheme 2 is a representation of how the current density ($j(x)$) might vary across the surface of a bipolar electrode. The total current density flowing through the electrode at each pole is the sum of the current densities along each pole (see eqs 3 and 4, for the cathodic and anodic poles, respectively).

$$i_c = w\int_0^{x_0} j(x)\,dx = w\int_0^{x_0} j(\eta_{(x)})\,dx \qquad (3)$$

$$i_a = w\int_{x_0}^{l_{elec}} j(x)\,dx = w\int_{x_0}^{l_{elec}} j(\eta_{(x)})\,dx \qquad (4)$$

Here, w is the width of the bipolar electrode. Finally, because electroneutrality must be satisfied across the bipolar electrode, the absolute values of the anodic and cathodic currents are equal ($i = -i_c = i_a$).

Solution Potential Difference between the Ends of the Electrode. There is no direct method for measuring the difference in solution potential between the two ends of a bipolar electrode. However, this problem can be addressed indirectly by measuring the potential using an alternative electrode design, which is compared with a standard bipolar electrode in the inset of Figure 2. In essence, the middle portion of the bipolar electrode is removed in the alternative design, leaving behind two 100-μm-

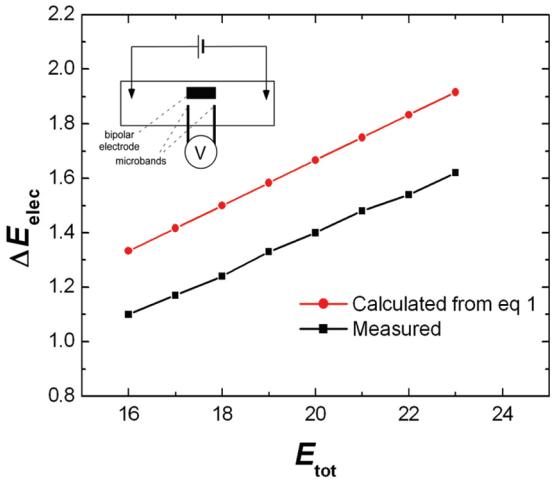

Figure 2. Plot of the difference in potential between two microbands (inset, ΔE_{elec}) as a function of the applied driving voltage (E_{tot}). This value corresponds to the total overpotential between the two ends of a continuous bipolar electrode. The solution contained 5.0 mM $Ru(bpy)_3^{2+}$ and 25.0 mM TPrA in 0.100 M phosphate buffer (pH 6.9). The inset shows an illustration of the experimental setup used to perform these measurements (see text for details).

wide microband electrodes separated at their outer edges by 1.00 mm. This distance is the same as the length of the continuous bipolar electrode. Note that the gold microbands extend beyond the channel, which makes it possible to connect a voltmeter between them and measure the potential difference (equivalent to ΔE_{elec}) as a function of E_{tot}. The results of this experiment are provided in Figure 2.

It is important to note that current cannot flow through the voltmeter or the microbands in this experiment. This implies that faradic reactions cannot occur at the microbands and, therefore, do not induce depolarization, which is a local decrease of the electric field in the solution over the bipolar electrode. In the case of a single, continuous bipolar electrode (top design, Figure 2 inset), depolarization occurs when the ionic current through the solution is low, compared to the faradaic current passing through the bipolar electrode.[12] In other words, the extent of depolarization will be dependent on the fraction of the total current that is carried by the bipolar electrode. The important point is that the two electrode configurations represented in the inset of Figure 2 are analogous, because even in the case of a single, continuous bipolar electrode, there is little depolarization. This is because the buffer concentration is always kept high. Experiments discussed later show that, under these conditions, ~99% of the current passes through the solution and just ~1% through the electrode.

The experimental results shown in Figure 2 can be compared to a calculated value by combining the geometrical arguments expressed in eq 1. This equation is plotted as the red line in Figure 2. The results indicate that the measured value of ΔE_{elec} is less than the calculated value. We conclude that the true potential drop across the channel is less than the drop between the two driving electrodes. That is, a portion of the applied potential E_{tot} is lost at the driving electrode/solution interface or within the reservoirs at either end of the channel. The potential difference between the two lines in Figure 2 suggests that ~3 V of E_{tot} are dropped outside the microfluidic channel. Qualitative confirmation of this speculation comes from the observation of ECL emission from the positive driving electrode. An ideal experimental configuration would employ infinitely narrow microbands for the measurement of ΔE_{elec}, because some potential will be dropped across the microbands. This will result in an underestimation of ΔE_{elec}. We have chosen to use microbands that have a width of just 100 μm to minimize this error.

Estimation of the Current Flowing through the Bipolar Electrode. In their seminal paper, Duval et al. predicted the current flow in a bipolar electrode.[11] Their elucidation of the Butler−Volmer equations for the anodic and cathodic processes led directly to the determination of x_0, as a function of the applied electric field. The determination of x_0 is then sufficient to establish a complete linear relationship between distance and overpotential (eq 2). Therefore, when eq 2 is combined with Butler−Volmer equations, it is possible to establish the current density profile $j(x)$. Finally, direct mathematical integration of an expression for $j(x)$ over the area of each pole leads to the value of the current (see Scheme 2). However, Duval's prediction is only valid when the electron-transfer kinetics of the faradaic reactions that are occurring on the bipolar electrode are explicitly known. In our system, this is not the case, and the complexity of the redox processes (oxygen and water reduction at the cathode and $Ru(bpy)_3^{2+}$ and TPrA oxidation at the anode) hinders our ability to define the reaction kinetics. Therefore, we are forced to determine $j(x)$ semiempirically.

The first step necessary for determining $j(x)$ was to empirically measure the current density versus stepped potentials ($j(E_{step})$) for an electrode contained within an air-saturated $Ru(bpy)_3^{2+}$/TPrA solution. This experiment was executed by configuring a traditional three-electrode cell within a microfluidic device, and then conducting a series of chronoamperometric experiments. Specifically, the fluidic system was filled with solution, the potential of a gold microband electrode situated near one of the reservoirs was stepped to different potentials, E_{step} (versus a reference electrode), and the resulting current transient was measured. Further details about this experiment are provided in Figure S1 of the Supporting Information. The data, which is a plot of j as a function of E_{step}, are provided in Figure 3.

We now focus on extracting $j(x)$ from $j(E_{step})$. This transition requires several steps. First, we converted $j(E_{step})$ to a secondary plot of current density versus overpotential, $j(\eta_{(x)})$ (top axis of Figure 3). This is accomplished by defining an equilibrium potential, E_{zcd} (where zcd denotes zero current density), in the $j(E_{step})$ plot. E_{zcd} is comparable to E_{elec} derived from the plot of $j(\eta_{(x)})$. This equivalence between E_{zcd} and E_{elec} establishes a reference point for converting $j(E_{step})$ to $j(\eta_{(x)})$ (see Figure 3). A rigorous mathematical explanation of this conversion is provided in the Supporting Information.

The conversion of $j(\eta_{(x)})$ to $j(x)$ requires a simple conversion of the η-axis to values of x using the linear relationship in eq 2. Unfortunately, eq 2 contains an unknown value, x_0, which must be derived mathematically before $j(\eta_{(x)})$ can be converted to $j(x)$. We describe the mathematical derivation of x_0 in the Supporting Information and calculated values of x_0 for several driving voltages are listed in Table 1. With x_0 known, it is possible to determine $j(x)$ and then determine the amount of

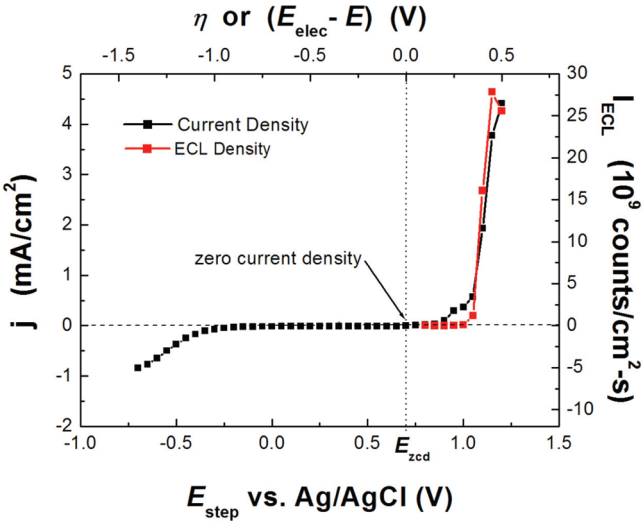

Figure 3. Current density (j) and ECL emission density (I_{ECL}) measured at a microband electrode. The solution contained 5.0 mM $Ru(bpy)_3^{2+}$ and 25.0 mM TPrA in 0.100 M phosphate buffer (pH 6.9). These measurements were obtained using a standard three-electrode cell (see Figure S1 in the Supporting Information). The bottom axis represents the potential of the working electrode versus Ag/AgCl, and the top axis represents the overpotential measured from the zero current density (ZCD) point.

Table 1. Calculated Values of Key Parameters, as a Function of the Applied Driving Voltage

E_{tot} (V)	ΔE_{elec} (V)	η_c (V)	η_a (V)	x_0 (mm)	i_a (nA)	E_{elec} (V)	ECL intensity (counts)
16.0	1.10	−0.90	0.20	0.82	20	7.7	
17.0	1.17	−0.95	0.22	0.81	27	8.2	
18.0	1.24	−0.99	0.25	0.80	34	8.7	
19.0	1.33	−1.06	0.27	0.79	44	9.2	6617
20.0	1.40	−1.10	0.30	0.79	54	9.7	13763
21.0	1.48	−1.16	0.32	0.78	70	10.2	48024
22.0	1.54	−1.20	0.34	0.78	89	10.7	136457
23.0	1.62	−1.26	0.36	0.78	117	11.2	374859

[a] Only ΔE_{elec} was measured. The parameters η_c and η_a are determined by the resolution of eqs S11 and S12 in the Supporting Information, x_0 is from eq S13 in the Supporting Information, i is determined from graphical integration of the linear current density, E_{elec} (see eq S3 in the Supporting Information), and the ECL intensity is determined from graphical integration of the linear ECL density.

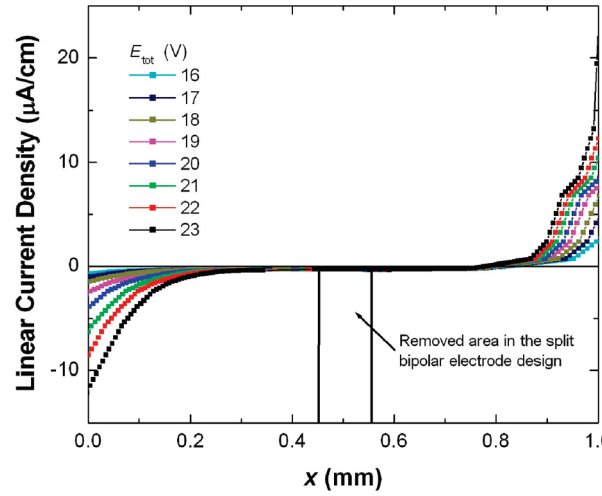

Figure 4. Linear current density as a function of position along a bipolar electrode for different values of the applied driving voltage (E_{tot}). The solution contained 5.0 mM $Ru(bpy)_3^{2+}$ and 25.0 mM TPrA in 0.100 M phosphate buffer (pH 6.9).

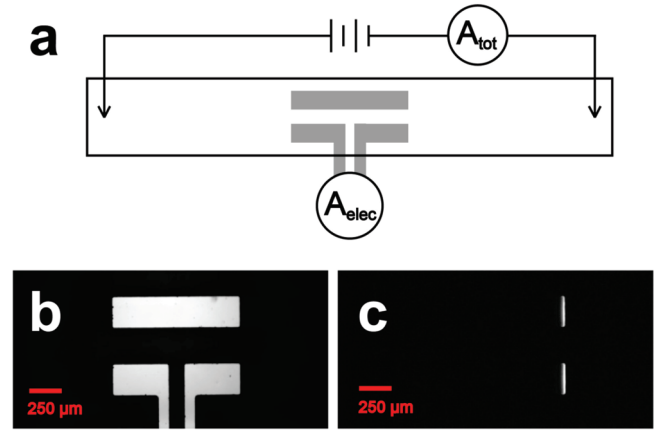

Figure 5. (a) Schematic representation of the experimental configuration used to quantify the extent of depolarization. (b) Optical micrograph of the electrode configuration corresponding to panel a. (c) Luminescence micrograph for E_{tot} = 22 V. The ECL intensities from the continuous and split bipolar electrodes were 0.19 and 0.22 × 10^6 counts, respectively. The solution contained 5.0 mM $Ru(bpy)_3^{2+}$ and 25.0 mM TPrA in 0.100 M phosphate buffer (pH 6.9).

current flowing through the bipolar electrode as a function of E_{tot}. The current density will be the same along the width of the electrode. Therefore, the linear current density, which is simply $j(x) \cdot w$ (where w is the width of the bipolar electrode), represents the total current density at a given position x along the length of the electrode. A series of linear current density plots, $j(x) \cdot w$ vs x, for different values of E_{tot}, are provided in Figure 4. Finally, graphical integration of the linear current density curves yields a predicted current value through the bipolar electrode for a specific applied driving voltage. Several calculated current values are listed in Table 1.

Direct Measurement of the Current at a Split Bipolar Electrode. To directly compare the currents calculated in the previous section to experimental measurements, the two halves of a split bipolar electrode design are connected by an ammeter (see Figure 5a).[7,8] This provides direct measurement of the electric current induced in the bipolar electrode by the two driving electrodes. The results in Figure 4 show that there is little or no faradaic electron transfer in the center of a bipolar electrode, which suggests that the electrochemical properties of the split electrode should be the same as a continuous bipolar electrode. However, to confirm the congruency of the split and continuous bipolar electrodes experimentally, one of each design was placed side by side in the same channel during every experiment (see Figure 5b), and the ECL emission from each was measured. As shown in Figures 5a and b, the outermost edge-to-edge length (l_{elec}) of both types of electrodes was the same. Note that the connections to the split electrode are placed at the inner edge of each half electrode, to ensure that faradaic reactions only occur at the ends of the electrode (and not on the contacts). The ECL emission from luminescence micrographs, such as that shown in Figure 5c, have been quantified using digital imaging software. Figure 6 compares the ECL intensities from split and continuous bipolar electrodes for different driving voltages, showing that the

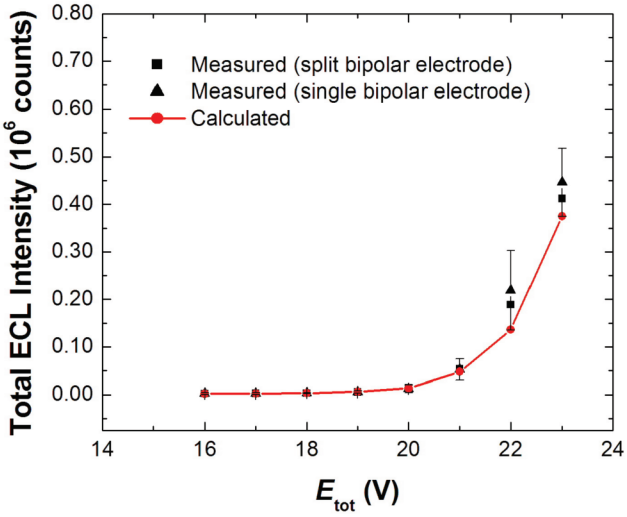

Figure 6. Simultaneous measurement of the total ECL intensity for both split and continuous (single) bipolar electrodes, as a function of the driving potential (E_{tot}). The measured values represent the average of four independently prepared devices. The red line represents the total ECL intensity estimated from the integration of the calculated ECL profiles.

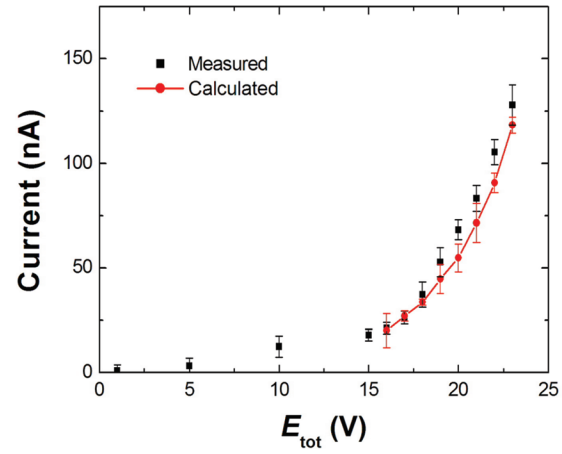

Figure 7. Plot of the current for a split bipolar electrode versus the applied driving potential (E_{tot}). The calculated values (data from Table 1, represented by the red curve) are averages from the integration of the current density over both cathodic and anodic poles, respectively. The error bars represent the standard deviation. The solution contained 5.0 mM $Ru(bpy)_3^{2+}$ and 25.0 mM TPrA in 0.100 M phosphate buffer (pH 6.9).

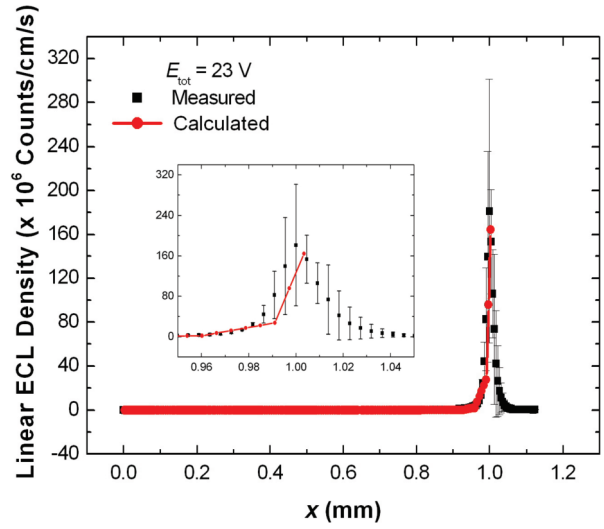

Figure 8. Plot of the linear ECL emission density for a bipolar electrode, as a function of position along the electrode. The inset shows an expanded view of the peak. The solution contained 5.0 mM $Ru(bpy)_3^{2+}$ and 25.0 mM TPrA in 0.100 M phosphate buffer (pH 6.9).

ECL intensity for the two designs is similar (always within 10% of each other). Moreover, when the direct connection (via a copper wire) between the two halves of the split electrodes is replaced by an ammeter (see Figure 5a), the correspondence of the ECL emission is maintained. A second ammeter may be connected between a driving electrode and the power supply, to measure the total current through the system (see Figure 5a). For E_{tot} = 20 V, the total current is ~65 μA, compared to 54 nA measured through the split bipolar electrode. The ratio of these two measured values indicates that the electric field will decrease <1% over the bipolar electrode and that the effects of depolarization are negligible. These results prove that the split design is equivalent to a continuous bipolar electrode, and that the split design can be used to directly measure the current passing through a bipolar electrode.[8]

In Figure 7, a plot of the current measured through a split bipolar electrode versus the voltage applied across the channel (E_{tot}) is compared to the current calculated using Figure 4. The close agreement between calculated and measured values suggests that the assumptions used for the calculations are valid. Recall that a particularly important postulate was that the potential drop over the length of the electrode is linear, and, thus, the effect of depolarization negligible, under the conditions used for these experiments.

Determination of the ECL Intensity Profile and the Total ECL Intensity. Just as the current density profile (Figure 4) can be semiempirically determined, the ECL density profile $I_{ECL}(x)$ can also be estimated using $\eta(x)$. This is done as follows. First, the ECL density is measured as a function of step potential, $I_{ECL}(E_{step})$, using the method used to generate the results in Figure 3 (see Figure S1 in the Supporting Information). Second, using the approach described earlier for the current density, the empirically determined ECL density, $I_{ECL}(E_{step})$, was used to generate a plot corresponding to $I_{ECL}(\eta)$. The results of these first two steps are displayed as the red line in Figure 3. Third, the values of $I_{ECL}(\eta)$ and $\eta(x)$ were used to determine $I_{ECL}(x)$ for different values of E_{tot}.

In contrast to the current density profile, the ECL profile can easily be measured directly. Figure 8 represents both measured and calculated ECL intensity profiles for E_{tot} = 23.0 V. The correspondence between the measured and calculated values of the ECL is striking, and both indicate that (at this driving potential) the overpotential required to drive the ECL reactions is only found at the end of the bipolar electrode.

Integration of the ECL density profile (Figure 8) leads to the total intensity of light observed at the bipolar electrode. Figure 6 compares the measured intensities for the two electrode designs with the integration of calculated ECL density profiles as a function of E_{tot}. The calculated intensities are, on average, slightly less than the

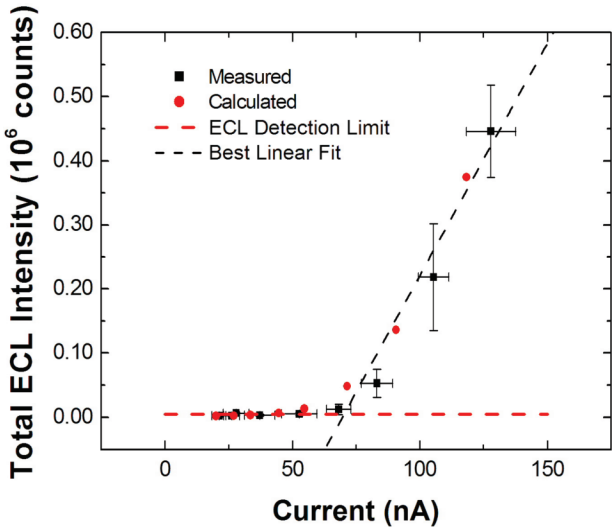

Figure 9. Relationship between the total ECL intensity and the faradaic current; the measured values represent the average of four independently prepared devices. The black points represent the total ECL intensity for a split bipolar electrode as a function of the measured current. The dashed red line is the ECL detection limit calculated from the measured value of the background noise plus three times the standard deviation on this measurement. The black dashed line is the best fit for the linear portion of the curve.

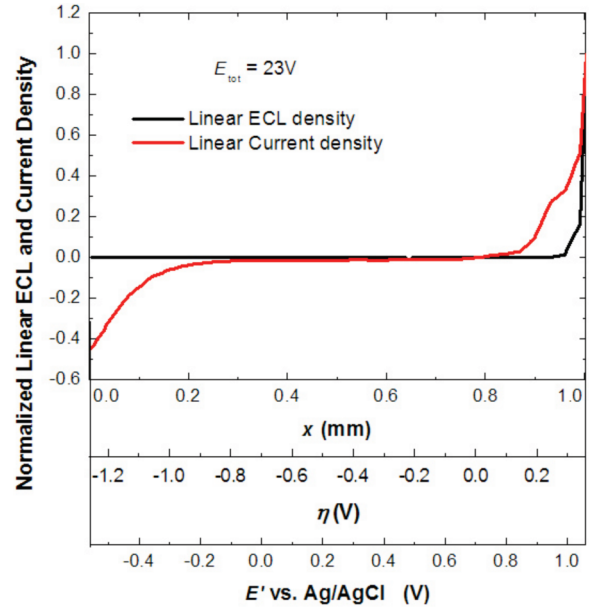

Figure 10. Normalized calculated linear ECL and current densities for $E_{tot} = 23.0$ V as a function of distance along the bipolar electrode, the overpotential, and the potential versus a Ag/AgCl reference electrode.

measured values; nevertheless, the correspondence between the measured and calculated intensities is quite satisfactory.

Relationship between the Faradaic Current and the ECL Intensity. Figure 9 shows the relationship between the total ECL intensity and the faradaic current. A key point is that, for our measurement system, a threshold current of ~75 nA must be attained before ECL is detected. Thereafter, the ECL intensity increases linearly as a function of the faradaic current. This linear relationship indicates that (i) ECL emission can be easily correlated to the faradaic current and, (ii) therefore, ECL emission will likely be useful as a reporter for quantitative sensing applications. The reporting sensitivity—that is, the amount of light emitted per unit of current flowing through the electrode—is easily calculated from the slope of the linear segment in Figure 9 (dashed black line). Under the conditions used in our experiments, the reporting sensitivity is ~7200 counts/nA.

From an analytical perspective, the threshold current governs the limit of detection for a species that is being reduced at the cathodic pole. Indeed, the reduction of an analyte must be able to produce a current that is higher than the threshold value before the ECL emission will reveal its presence. The lowest current density that can be indirectly detected through ECL reporting is ~32 μA/cm^2. This value was determined from the threshold current required for detection of ECL and the surface area of the bipolar electrode.

The presence of the threshold current means that faradaic reactions that do not produce detectable light occur at the bipolar electrode at low overpotential. It is well-established that the principal pathway for ECL emission at high concentrations of $Ru(bpy)_3^{2+}$ (>500 μM) involves the catalytic, homogeneous cross reaction between $Ru(bpy)_3^{3+}$ and TPrA. However, a separate pathway involving direct TPrA oxidation at the electrode surface also occurs competitively at pH >6.[19−21] Both pathways require direct oxidation of $Ru(bpy)_3^{2+}$ at the electrode surface, but the direct oxidation of TPrA occurs at a lower potential than $Ru(bpy)_3^{2+}$ oxidation on gold electrodes. The important point is that, under the conditions used in our experiments, TPrA oxidizes before $Ru(bpy)_3^{2+}$, but direct oxidation of $Ru(bpy)_3^{2+}$ is required to detect ECL. These considerations correlate with our experimental finding that current is observed at the bipolar electrode at potentials where no ECL is detected. That is, this pre-ECL current may be attributable to the oxidation of TPrA prior to the onset of $Ru(bpy)_3^{2+}$ oxidation.[21]

In addition to the representation shown in Figure 9, the threshold faradaic current can also be visualized by overlaying the linear ECL and current density profiles (see Figure 10). For example, at $E_{tot} = 23.0$ V, a region of the electrode, ranging from 0.86 to 0.96 mm, is observed where there is significant faradaic current but no detectable ECL emission. Significantly, the difference in overpotential between the onset of faradaic current and the onset of ECL is similar to that usually observed for the oxidation of TPrA and $Ru(bpy)_3^{2+}$[20,21] (here, ~0.85 and 0.97 V vs Ag/AgCl, respectively, as noted on the potential scale of Figure 10). An alternative perspective is that the anodic overpotential (η scale in Figure 10) must attain a value of at least 0.3 V before ECL is detected. This means that the lowest analyte concentration that will result in light emission must be sufficiently large that the equilibrium potential taken by the bipolar electrode is high enough for at least 0.3 V to be dropped between x_0 and the far right end of the electrode l_{elec} (see Scheme 2).

(19) Gross, E. M.; Pastore, P.; Wightman, R. M. *J. Phys. Chem. B* **2001**, *105*, 8732–8738.
(20) Kanoufi, F.; Zu, Y.; Bard, A. J. *J. Phys. Chem. B* **2001**, *105*, 210–216.
(21) Miao, W. J.; Choi, J. P.; Bard, A. J. *J. Am. Chem. Soc.* **2002**, *124*, 14478–14485. (Note that a third ECL pathway, where only TPrA is oxidized at the electrode surface, occurs for solutions that contain micromolar concentrations of $Ru(bpy)_3^{2+}$ and, therefore, does not apply in our case.)

One way to increase the overpotentials on the anodic pole for a given driving voltage is to change the geometry of the electrode. Indeed, if the electrode area is reduced on its right side, more overpotential will be required to balance the cathodic processes at the other end. In other words, x_0 is shifted closer to the cathodic pole. This shift of x_0 forces the anodic overpotential, η_a, to increase. Therefore, the emission of light will occur for a lower bipolar current. Experimental evidence of this phenomenon has already been reported using a T-shaped electrode.[2]

SUMMARY AND CONCLUSIONS

Here, we have provided a theoretical framework for understanding analytical applications of bipolar electrodes and bipolar electrode arrays. Experimental confirmation of this framework has also been provided. The key findings are as follows. First, a semiempirical prediction of current flow through a bipolar electrode has been rigorously described. These results were successfully correlated to direct measurements of the total current for a split electrode system that mimics the behavior of a bipolar electrode. Second, a similar approach was used to calculate the electrogenerated chemiluminescence (ECL) emission profile along a bipolar electrode, and these predictions were confirmed experimentally. Third, ECL emission was related to the total amount of current flowing through the bipolar electrode and some conclusions concerning their relevance to chemical analysis were described.

Our attention is now focused on using the information reported here to fabricate large-scale bipolar arrays[22] and evaluate them for chemical sensing applications. In addition, we are learning how to improve the sensitivity and limit of detection for ECL reporting from bipolar electrodes by manipulating the geometry of the cell and electrodes, and by introducing additives to the buffer solution to reduce the overpotentials for ECL emission. Results from these experiments will be reported in due course.

ACKNOWLEDGMENT

The authors gratefully acknowledge financial support from the U.S. Army Research Office and the U.S. Defense Threat Reduction Agency (through Grant No. W911NF-07-1-0330). We also thank the Robert A. Welch Foundation (through Grant No. F-0032). E.S. thanks Prof. Robert Forster and the Irish Research Council for Science, Engineering and Technology for support under the Embark Initiative.

(22) Chow, K.-F.; Mavré, F.; Crooks, J. A.; Chang, B.-Y.; Crooks, R. M. *J. Am. Chem. Soc.* **2009**, *131*, 8364–8365.

MAJOR SYMBOLS

$\eta_{(x)}$ = difference in potential between the electrode and the solution at position x (V)
η_a = maximum anodic overpotential (V)
η_c = maximum cathodic overpotential (V)
ΔE_{elec} = potential difference between two ends of the bipolar electrode (V)
E_a = most negative solution potential over the bipolar electrode (V)
E_c = most positive solution potential over the bipolar electrode (V)
E_{elec} = equilibrium potential of the bipolar electrode (V)
$E_{l_{elec}/2}$ = potential of the solution at the halfway along the channel (V)
E_{zcd} = potential of zero net current density (V)
E_{tot} = applied potential difference between two driving electrodes (V)
E_{step} = potential of the working electrode in the three-electrode-cell potentiostep experiment (V)
i_a = anodic current (A)
i_c = cathodic current (A)
I_{ECL} = ECL emission density (counts/(cm^2 s))
j = current density (A/cm^2)
$j \cdot w$ = linear current density (A/cm)
$l_{channel}$ = length of the microchannel (mm)
l_{elec} = length of the bipolar electrode (mm)
P_a = power delivered at the anodic pole (A V/cm)
P_c = power delivered at the cathodic pole (A V/cm)
V_0 = electric field (V/cm)
w = width of the bipolar electrode (mm)
x = position on a bipolar electrode (mm)
x_0 = position on the bipolar electrode where the potential of the electrode and solution are equal (mm)

SUPPORTING INFORMATION AVAILABLE

Device fabrication procedures, determination and calculation of E_{elec}, three-electrodes cell experiments, conversion of $j(E_{step})$ to $j(\eta_{(x)})$, and rigorous determination of x_0 are provided. This material is available free of charge via the Internet at http://pubs.acs.org.

Received for review April 7, 2009. Accepted June 8, 2009.

AC900744P